JACS
JOURNAL OF THE AMERICAN CHEMICAL SOCIETY
Article
pubs.acs.org/JACS

Melting Thermodynamics of Reversible DNA/Ligand Complexes at Interfaces

Irina Belozerova and Rastislav Levicky*

Department of Chemical & Biomolecular Engineering, Polytechnic Institute of New York University, Brooklyn, New York 11201, United States

Supporting Information

ABSTRACT: A variety of solution methods exist for analysis of interactions between small molecule ligands and nucleic acids; however, accomplishing this task economically at the scale of hundreds to thousands of sequences remains challenging. Surface assays offer a prospective solution through array-based multiplexing, capable of mapping out the full sequence context of a DNA/ligand interaction in a single experiment. However, relative to solution assays, accurate quantification of DNA/ligand interactions in a surface format must contend with limited understanding of molecular activities and interactions at a solid−liquid interface. We report a surface adaptation of a solution method in which shifts in duplex stability, induced by ligand binding and quantified from melting transitions, are used for thermodynamic analysis of DNA/ligand interactions. The results are benchmarked against solution calorimetric data. Equilibrium operation is confirmed through superposition of denaturation/hybridization transitions triggered by heating and cooling. The antibiotic compound netropsin, which undergoes electrostatic and sequence-specific minor groove interactions with DNA, is used as a prototypical small molecule. DNA/netropsin interactions are investigated as a function of ionic strength and drug concentration through electrochemical tracing of surface melt transitions. Comparison with solution values finds excellent agreement in free energy, though reliable separation into enthalpic and entropic contributions proves more difficult. The results establish key guidelines for analysis of DNA−ligand interactions via reversible melting denaturation at surfaces.

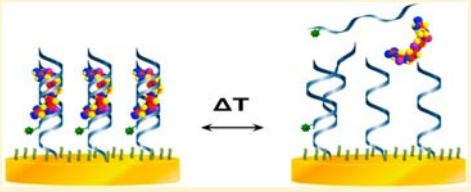

1. INTRODUCTION

Interactions between small molecule ligands and nucleic acids appear in many contexts including design of small molecule transcription regulators[1−5] and DNA dyes and drug potentiators,[4,6,7] tools for toxicological screens,[8−11] and DNA-targeted therapy including anticancer, antibiotic, antiviral, and antitrypanosomal compounds.[12−16] Most DNA/ligand interactions are sensitive to the base sequence of the nucleic acid; therefore, to understand the recognition mechanisms, it is necessary to establish the sequence dependence. This task can be complicated by the large number of sequences that may need to be screened for ligand-binding affinity, possibly ranging into thousands of interactions.

In principle, multiplexed analysis of interactions between small molecules and nucleic acids can proceed by parallelization of classical methods such as calorimetry, denaturation, or footprinting assays. For example, advances in array calorimetry are leading to reductions in sample requirements and faster times to result, though significant hardware challenges remain.[17] Very highly scalable approaches have also appeared.[18−24] Techniques based on "fluorescent intercalator displacement" (FID) have been implemented in microwell[18,20] as well as microarray[21] formats; the microarray format enabled analysis of over 1×10^5 interactions. In FID, binding of the ligand of interest displaces an intercalated fluorophore, such as ethidium bromide, from the nucleic acid, causing a change in fluorescence. Other approaches have relied on tagging the small molecule with a fluorophore,[22,23] or on monitoring binding through the force required to separate the two strands of a duplex in the presence of the small molecule.[24] Many of these advances have exploited the excellent high-throughput capacity, and frugal reagent consumption, of microarrayed supports.

A central difficulty with most existing multiplexed approaches, however, is that the measurement tends to complicate the interaction. FID employs a competitive displacement format in which an intercalating agent is introduced to the DNA in advance of small molecule binding; in this case, energetics of displacement of the intercalator can suppress detection of weaker associations.[18] If, instead, the small molecules are fluorescently labeled, the measured affinities can differ from those of the unlabeled species.[23] Additionally, some methods require washing and/or drying of the sample prior to measurement;[21,22] in these instances, the binding equilibrium is perturbed, thus placing thermodynamic analysis on uncertain grounds. Approaches based on in situ label-free methods, such as surface plasmon resonance (SPR)[25−30] or quartz crystal microbalance (QCM) techniques,[31,32] avoid many of these difficulties. However, these alternate methods can be challenging and costly to scale up to high-throughput, and they are susceptible to nonspecific background signals as they do not track a signal specific to

Received: July 7, 2012
Published: October 9, 2012

   dx.doi.org/10.1021/ja3066368 | J. Am. Chem. Soc. 2012, 134, 18667−18676

Table 1. Oligonucleotide Sequences and Purpose

base sequence (5′ to 3′)	abbreviation	purpose
GGA ATT GGC TTTTT-$(CH_2)_3$-SS-$(CH_2)_3$OH	PI	probe for melting assays on solid supports
NH_2-$(CH_2)_6$-GCC AAT TCC	CPI	complementary strand for melting assays on solid supports
GGA ATT GGC TTTTT	PF	probe for calorimetric studies; same base sequence as PI
GCC AAT TCC	CPF	complementary strand for calorimetric studies

the interacting molecules, but rather monitor changes in global properties (e.g., refractive index for SPR, mass for QCM) at the sensor surface. Baseline stability and corrections for variability in refractive index increments (SPR) or sequestered solvent (QCM) can be additional complications.

Distinct from above approaches, denaturation assays are built on the biophysical principle that preferential binding of small molecules to double-stranded relative to single-stranded structure will shift denaturation thresholds, such as melting temperatures. This effect has been exploited in solution to derive thermodynamics of DNA/ligand associations from melting curve analysis.[33−36] Adaptation of denaturation assays to a highly scalable surface format would be especially promising because this approach (i) avoids labeling of the small molecule, thus preempting biasing of the interaction by presence of a label; (ii) is only sensitive to those small molecules that associate with DNA, thereby providing immunity to nonspecific adsorption of the ligand; (iii) operates *in situ*, without the need to wash or dry the sample, thus binding equilibria are not perturbed prior to measurement; and (iv) for reversible DNA/ligand associations, can verify equilibrium through superposition of heating and cooling traces.

This report describes initial validation of surface denaturation assays for thermodynamic analysis of DNA/small molecule ligand interactions at the level of a test site, with the aim to validate prospects for future integration in parallelized (e.g., microarray) platforms. Optimization of melting measurements for tethered duplexes is described, and the approach is used to determine thermodynamics of binding between a model compound, netropsin (Net), and its DNA recognition site. Net is a minor-groove binder with high specificity for double-stranded DNA sequences rich in adenine-thymine base pairs[37,38] whose fundamental properties continue to be investigated,[39−42] although toxicity renders it unsuitable for clinical use.[37] Net-DNA interactions are studied as a function of ionic strength and ligand concentration by electrochemically monitoring melting transitions of immobilized duplexes. Compared to optical methods requiring generation and detection of light, electrochemical detection simplifies portable integration and, in a commercial setting, could leverage recent progress in electrochemical microarrays.[43−47] Values of free energy, enthalpy, and entropy derived from experiments on solid supports are compared to those from isothermal titration calorimetry (ITC) solution studies. A coupled-equilibria model accounting for three immobilized species including single-stranded "probes", double-stranded "duplexes" without Net, and Net-duplex "complexes" is used for analysis of the melting transitions. The results demonstrate feasibility of surface denaturation assays for quantitative, scalable analysis of interactions between small molecules and nucleic acids.

2. MATERIALS AND METHODS

2.1. Materials. Table 1 lists the oligonucleotide sequences used. All oligonucleotides were HPLC-purified by the provider (Eurofins MWG Operon). Probe oligonucleotide for immobilization, PI, contained a 3′ disulfide for surface attachment and a five-thymine "spacer" to provide elevation above the solid support and improve accessibility for hybridization with the complementary strand CPI. The CPI oligonucleotide contained a 5′ amine for electroactive labeling with *N*-succinimidyl ferrocenecarboxylate (FcCA-NHS, TCI America). Labeling reactions were performed overnight at room temperature by combining 300 μL of 33 μmol L^{-1} solution of CPI in 0.2 mol L^{-1} pH 9 sodium carbonate buffer with 60 μL of 82 mmol L^{-1} solution of FcCA-NHS in dimethyl sulfoxide. Unreacted FcCA-NHS was removed on a NAP 10 column (GE Healthcare), and the FcCA-labeled CPI was further purified via reverse-phase HPLC (Beckman Coulter Gold 125; Phenomenex Clarity 3 μm Oligo-RP C18 column). HPLC was performed at room temperature with a linear gradient of 12−65% acetonitrile in 0.1 mol L^{-1} triethylamine acetate, pH 7.0, at a flow rate of 0.5 mL min^{-1} over 25 min. The collected, FcCA-labeled DNA, hereafter referred to as FcCA-CPI, was dried (Vacufuge, Eppendorf) and stored at −20 °C.

The PF probe, and its complementary sequence CPF, were used for solution ultraviolet spectroscopy and ITC experiments. Netropsin was purchased from Santa Cruz Biotechnology, Inc.

Oligonucleotide concentrations were determined using absorbance at 260 nm and supplier-provided extinction coefficients. Netropsin concentrations were measured at 296 nm, based on a molar extinction coefficient of 21 500 M^{-1} cm^{-1}.[48,49]

2.2. Sample Preparation. PI monolayers were prepared on 3 mm diameter gold rotating disk working electrodes (Bioanalytical Systems, Inc.). Prior to layer formation, electrodes were mechanically polished with 1 μm diamond suspension, sequentially sonicated for 3 min in methanol and water, further mechanically polished with 0.3 μm alumina, and recleaned with sonication in methanol and water. The mechanical treatment was immediately followed by electrochemical polishing consisting of 10 cycles from −0.2 to 1.75 V at 0.1 V s^{-1} in 0.5 mol L^{-1} sulfuric acid with 10 mmol L^{-1} potassium chloride, followed by 50 cycles in 0.5 mol L^{-1} sulfuric acid. All electrode potentials are expressed relative to an Ag/AgCl/3 mol L^{-1} NaCl reference electrode. Surface reproducibility was assessed from superimposition of subsequent scanning cycles. Electrodes were rinsed with deionized water (18.2 MΩ cm) and the roughness factor, defined as the ratio between actual and geometric areas of the electrode, was determined from double layer capacitance in 0.1 mol L^{-1} sodium fluoride at −0.84 V.[50] The electrode surface was kept wetted at all times to minimize surface contamination.

PI monolayers were formed by immersing cleaned electrodes in 0.5 mol L^{-1} pH 7 sodium phosphate buffer (SPB) containing 2 μmol L^{-1} PI probe for 90 min. Following PI immobilization, electrodes were passivated with 6-mercapto-1-hexanol (MCH) (Sigma-Aldrich) to block nonspecific adsorption of DNA and to assist extension of probe chains above the solid support.[51,52] Passivation was realized by immersion of PI-modified electrodes in 1 mmol L^{-1} MCH solution in 0.1 mol L^{-1} pH 7 SPB for 90 min. Both probe immobilization and MCH passivation were performed at 45 °C. Compared to immobilization at room temperature, preparation at 45 °C was found to improve stability of the monolayers during melting curve measurements.

2.3. Electrochemical Measurement of Surface Melting Transitions. Melting experiments were performed in 150, 345, or 790 mmol L^{-1} sodium perchlorate, with each solution in addition containing 100 μmol L^{-1} MCH and 2 mmol L^{-1} pH 7 SPB. These three buffers will be referred to as SP150, SP345, and SP790, respectively. Presence of mercaptohexanol in solution maintained

dx.doi.org/10.1021/ja3066368 | J. Am. Chem. Soc. 2012, 134, 18667−18676

surface passivation by replacing any MCH that may have desorbed during measurement. For determination of melting transitions, complementary FcCA-CPI strands were added to a 26 nmol L^{-1} concentration. All solutions were deoxygenated by nitrogen bubbling for 20 min prior to initiating experiments, and a nitrogen blanket was maintained throughout measurement.

A melting cycle consisted of cooling from 45 to 6 °C, followed by reheating to 45 °C. During the cooling ramp, FcCA-CPI from solution hybridized with the PI monolayer to form PI-CPI duplexes, while heating cycles melted the duplexes to release FcCA-CPI strands back into solution. Temperature scan rates were sufficiently slow to ensure proximity to thermodynamic reversibility. As discussed further below, maximal scan rates compatible with near reversible operation varied with ionic strength, being about 0.17 °C min^{-1} in SP150, 0.25 °C min^{-1} in SP345, and 0.36 °C min^{-1} in SP790. For analysis of Net–DNA interactions, two melting cycles were performed on each layer: a first cycle without Net, and a second cycle at the start of which the electrode was immersed in a fresh solution of FcCA-CPI with Net added at a concentration of either 5, 50, 500, or 2000 nmol L^{-1}.

Melting transitions were monitored electrochemically from the surface coverage of FcCA-CPI strands. Measurements were performed on a CHI 440A workstation (CHI Instruments) using a rotating disc working electrode (RDE) at 1500 rpm, modified as described in section 2.2, a platinum wire counter electrode, and a silver/silver chloride reference electrode (Ag/AgCl/3 mol L^{-1} NaCl). The RDE setup facilitated mass transport of complement strands and Net to the probe layer. The reference electrode was inserted into a glass sleeve with a porous frit to create a double liquid junction as a precaution against leakage of electrolyte from the reference electrode reservoir into the sample buffer. Cyclic voltammetry (CV) scans were collected at 20 V s^{-1}. The working electrode was kept at 0 V between CV measurements.

Figure 1 is an example of CV series for a cooling–heating cycle (for clarity, not all temperatures are shown). The FcCA redox peaks at

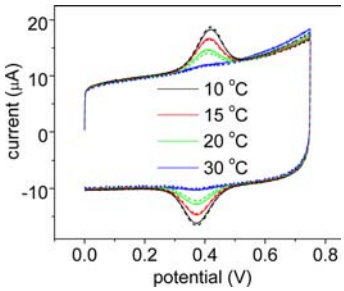

Figure 1. Examples of CV traces measured during cooling (solid curves) and heating (dashed curves) portions of a melting cycle. The FcCA peak at 0.4 V monitors hybridization of FcCA-CPI strands, which were present at 26 nmol L^{-1} in SP150.

around 0.4 V increase with decreasing temperature during cooling (solid curves), indicating hybridization of CPI strands to the PI monolayer, with reverse behavior observed during heating (dashed curves). Using previously described algorithms,[53] the peak areas were integrated to derive the total surface coverage S_{Dtot} of PI-CPI duplexes as a function of temperature T. Melting curves were created by plotting S_{Dtot} versus T.

2.4. UV–vis Spectroscopy and Solution Melting. Solution melting data were obtained on a Cary 50 UV–vis spectrophotometer (Agilent Technologies) equipped with a temperature-controlled single cuvette accessory (Quantum Northwest Inc.). Solutions containing 0.5 μmol L^{-1} each of PF and CPF in 150 mmol L^{-1} sodium perchlorate buffered at pH 7 with 2 mmol L^{-1} SPB were heated from 15 to 65 °C at 0.2 °C min^{-1}, with a 10 min wait at terminal temperatures to confirm equilibration. Solution melting of PI–CPI duplexes was compared with the corresponding surface process.

2.5. Isothermal Titration Calorimetry of DNA/Net Association. Isothermal titration calorimetry (ITC) experiments were performed on a VP-ITC station (MicroCal, LLC) at 19.8 °C and in the same buffers (SP150, SP345, SP790) used for measurement of Net binding to immobilized duplexes, but without solution MCH. PF and CPF oligonucleotides were mixed at 5 μmol L^{-1} to form PF/CPF duplexes. Prior to experiments, the PF–CPF mixture was heated to 60 °C followed by slow cooling to room temperature in an incubation chamber to allow gradual formation of equilibrated DNA duplexes. The equilibrated duplex solution was loaded into the ITC sample cell, and 45 5-μL injections of 100 μmol L^{-1} netropsin solution were performed at 240 s intervals at a 502 rpm stirring speed. ITC data were analyzed using Origin 7.0 (OriginLab Corp.).

2.6. Modeling of Surface Melting Transitions. Thermodynamic analysis was performed by fitting of an equilibrium model to experimental data in OriginPro 8.5 (OriginLab Corp.). The use of an equilibrium model was justified by near reversible conditions of measurement, as confirmed from superposition of cooling and heating traces (see below). The model assumed that the DNA duplex is sufficiently short to possess a single binding site, that the small molecule ligand does not bind single-stranded DNA, and that the number of ligands binding per site (i.e., the binding stoichiometry) is fixed. These assumptions can be relaxed at the expense of additional model parameters; for example, Crothers and McGhee both describe situations when single- as well as double-stranded DNA interacts with ligands,[34,54] and illustrate how preferential binding for one over the other can be established from solution melting curves.

In the presence of the ligand L, three different states of immobilized DNA will coexist on the surface: single-stranded probes P, "free" duplexes D_{free} consisting of a probe and its complementary strand C, and "bound" duplexes D_{bound} complexed with n molecules of L, Figure 2. These states are connected by hybridization and binding equilibria,

$$P + C \leftrightarrow D_{free} \quad \text{(hybridization)}$$

$$D_{free} + nL \leftrightarrow D_{bound} \quad \text{(binding)}$$

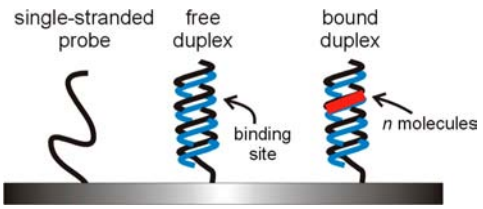

Figure 2. Possible states of a surface DNA site.

If C and L are present in excess, a condition met experimentally,[55] their solution concentrations can be treated as constant. The system can then by described by two equilibria and one conservation constraint,

$$K_H = \frac{S_{Dfree}}{(S_0 - S_{Dfree} - S_{Dbound})C_C} \quad (1)$$

$$K_B = \frac{S_{Dbound}}{S_{Dfree}C_L^n} \quad (2)$$

$$S_0 = S_P + S_{Dfree} + S_{Dbound} \quad (3)$$

where K_H and K_B are equilibrium constants for DNA hybridization and DNA/Net binding, respectively. The equilibrium constants follow from the corresponding standard enthalpies and entropies (R, gas constant; T, absolute temperature)

$$K_H = \exp\left[-\frac{(\Delta H_H^\circ - T\Delta S_H^\circ)}{RT}\right] \quad (4)$$

$$K_B = \exp\left[-\frac{(\Delta H_B^\circ - T\Delta S_B^\circ)}{RT}\right] \quad (5)$$

dx.doi.org/10.1021/ja3066368 | J. Am. Chem. Soc. 2012, 134, 18667–18676

The other parameters include the surface coverages for the three states, S_P, S_{Dfree}, and S_{Dbound}; the total coverage S_0 of immobilized strands; and the solution concentrations C_C and C_L of complementary strands and small ligands, respectively. Subscript H denotes quantities describing probe-complement hybridization, while B denotes those associated with ligand binding.

Solving eqs 1−3 for S_P, S_{Dfree}, and S_{Dbound} in terms of the other parameters leads to the total duplex coverage, $S_{Dtot} = S_{Dfree} + S_{Dbound}$,

$$S_{Dtot} = S_0 \frac{K_H C_C (1 + K_B C_L^n)}{1 + K_H C_C (1 + K_B C_L^n)} \quad (6)$$

In absence of the small molecule, $C_L = 0$, eq 6 reduces to the familiar Langmuir isotherm

$$S_{Dtot} = S_0 \frac{K_H C_C}{1 + K_H C_C} \quad (7)$$

Equations 6 and 7 were fit to experimental melting curves, that is, to measured S_{Dtot} as a function of temperature, by optimizing the unknowns S_0, ΔH_H°, ΔS_H°, ΔH_B°, and ΔS_B°. As described earlier, two melting transitions, a first cycle in absence of Net followed by cycle II with the drug, were measured for each set of conditions. Equation 7 was fit to cycle I data while eq 6 was used for cycle II. Although algorithms are available for predicting hybridization thermodynamics in solution (e.g., ref 56), these were not used to predict the ΔH_H° and ΔS_H° of surface hybridization because of well documented disparities between the solution and surface processes (e.g., see refs 57−60). Among other surface specific effects, surface hybridization depends on organization of the DNA monolayer. This organization varies as densities of single- and double-stranded species change, and hence, with position along a melting curve. For this reason, ΔH_H° and ΔS_H° are also expected to vary as melting proceeds because the physical characteristics of the layer, such as its charge density,[61−66] change. Modeling of such effects, however, is challenged by substantial uncertainties about layer organization. Therefore, instead, ΔH_H° and ΔS_H° were treated as effective averages characteristic of the entire melting transition. So long as the structure (e.g., minor groove) recognized by a small molecule does not depend significantly on organization of the greater layer, this approximation should not interfere with determination of ΔH_B° and ΔS_B°.

Another slightly subtle issue concerns the definitions of K_H and K_B in eqs 1 and 2. By expressing the equilibrium constants in terms of solution concentrations C_C and C_L, rather than the (unknown) surface concentrations of these species, the fitted thermodynamic functions will include contributions from partitioning of C and L between solution and the probe layer. If the partitioning costs are significant, they could bias the derived binding affinities. Partitioning of charged species, such as Net, is governed by electrochemical equilibria.[67] For a species j with signed valency z_j, solution concentration $C_{j,B}$, and local surface concentration $C_{j,S}$, the equilibrium condition can be approximated as (e.g., see ref [66])

$$\frac{ez_jV_S}{kT} = \ln\left(\frac{C_{j,B}}{C_{j,S}}\right) \quad (8)$$

where e is the elementary charge, V_S is the electrostatic potential difference between the surface and solution phases, and k is the Boltzmann constant. If V_S were known, the partitioning energy $E_{P,L}$ for the L ligand can be calculated from $E_{P,L} = z_L eV_S$ and its magnitude compared with experimentally derived binding energies. This comparison was performed by using eq 8 to calculate V_S from estimated concentrations of Na^+ at the surface. As described in the Supporting Information, the upper limit on $E_{P,Net}$ was only about 5% of the experimentally determined free energy of Net binding. As this percentage falls within experimental uncertainties it was not considered further.

3. RESULTS AND DISCUSSION

3.1. Reversibility of DNA Melting at Surfaces. For purposes of downstream analysis, it was important to establish whether experimental data refer to equilibrium. Melting measurements can validate equilibrium by comparing whether helix−coil transitions triggered by two different paths, cooling and heating, superimpose. Reversible operation can be enforced by ensuring that temperature ramp rates are sufficiently slow. This is illustrated in Figure 3A, which compares surface melting transitions for PI−CPI duplexes for "fast" 0.36 °C min^{-1} and "slow" 0.17 °C min^{-1} ramp rates, when immersed in SP150 buffer. The faster rate resulted in pronounced deviations between cooling and heating branches at lower temperatures; per contra, the two curves closely superimposed if the rate was lowered to 0.17 °C min^{-1}.

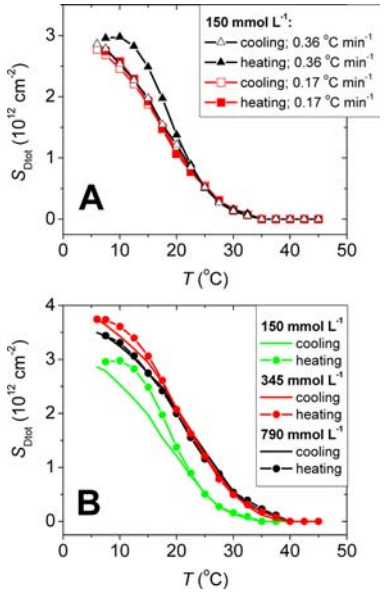

Figure 3. (A) Melting transitions for immobilized PI−CPI duplexes for two scan rates when immersed in SP150 buffer. (B) Melting transitions for a scan rate of 0.36 °C min^{-1}, under different concentrations of salt.

For a constant ramp rate, higher ionic strengths promoted faster equilibration, improving superposition of cooling and heating scans. This is illustrated in Figure 3B, where hysteresis at a scan rate of 0.36 °C min^{-1} in SP150 gradually disappeared as the sodium perchlorate concentration was raised to 790 mmol L^{-1}. This trend agrees with observations by Fuchs et al. who, using a 2 °C min^{-1} scan rate and 16mer probe sequences, found hysteresis for 157 mmol L^{-1} but not for 420 mmol L^{-1} or higher salt concentrations.[57] Moreover, closer inspection of Figure 3A reveals that cooling traces at the different scan rates superimposed, but the heating traces did not. Therefore, the hysteresis arose from slowness of dehybridization during melting, rather than from duplex formation during cooling. The observation that heating leads to greater hysteresis at low ionic strengths implies that dehybridization slows down as salt concentration decreases, a curious conclusion since increase in electrostatic repulsions between the strands of a duplex at low salt may be expected to assist, not hinder, strand separation. Origins of this behavior are not understood at present, but possibly reflect greater availability, at lower ionic strengths, of

dx.doi.org/10.1021/ja3066368 | J. Am. Chem. Soc. 2012, 134, 18667−18676

free probe nucleotides at surrounding sites that could interact with a dehybridizing CPI strand to slow down its departure.

On the basis of optimization of scan rates, subsequent experiments used the following conditions: 0.17 °C min^{-1} for SP150, 0.25 °C min^{-1} for SP345, and 0.36 °C min^{-1} for SP790 buffers. These conditions ensured near reversible behavior as illustrated in Figure 3A for the 0.17 °C min^{-1} data.

3.2. Monolayer Stability. A number of investigators noted the limited stability of monothiolate-anchored DNA strands on gold, and sought to develop more robust immobilization chemistries.[68−78] Melting transition measurements are especially demanding on such monolayers because of the use of elevated temperatures and necessarily slow scan rates to ensure reversible operation. The present study retained the simplicity of monothiolate immobilization while implementing two primary precautions to decrease monolayer degradation. First, monolayers were prepared at elevated temperatures (45 °C) to decrease the fraction of probes possibly anchored to less stable surface sites. Second, the duplex sequence, consisting of the binding site and G rich end-caps, was sufficiently short to place the melting transition near room temperature. Use of ∼10mer (or even shorter) sequences for study of small molecule binding is not particularly restrictive as many small molecules recognize base stretches of 6 bp or less.[79] Nucleic acid systems with higher melting temperatures could be accommodated in the future through one of the thermostable immobilization chemistries.[68−78]

Stability of DNA monolayers was evaluated by recording two consecutive cool-heat cycles, corresponding to four sequential stages of cooling 1 (C1), heating 1 (H1), cooling 2 (C2), and heating 2 (H2). After H1, the probe monolayer was switched into a fresh solution of complement to compensate for possible tag degradation;[80] therefore, any decrease in hybridization between the H1 and C2 stages should be attributed to loss of active probes from the surface. These stability tests, plotted in Figure 4, revealed that *within* a cycle the cooling and heating

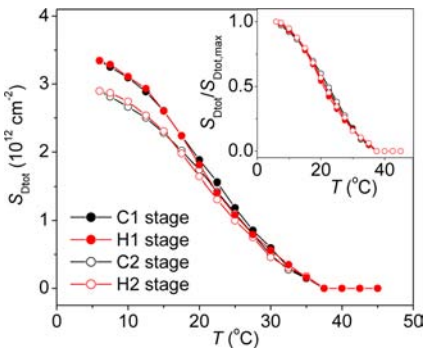

Figure 4. Main panel: Stability of probe layers to repeated temperature scanning, for a PI monolayer under 26 nmol L^{-1} solution of FcCA-CPI in SP345 buffer. Four transitions were measured in order: cooling #1 (C1), heating #1 (H1), cooling #2 (C2), and heating #2 (H2). Inset: Same data after normalization to maximum hybridization, $S_{Dtot,max}$.

traces (e.g., C1 and H1, C2 and H2) superimposed. In contrast, hybridization decreased by 10 to 15% between H1 and C2, when a heating stage was followed by a cooling stage. Similar results were obtained at all ionic strengths.

The observations derived from Figure 4 can be understood as follows. Comparison of two transitions within a cycle, when a cooling stage is followed by a heating stage, occurs without sampling the highest, most damaging, temperatures in between transitions. These traces therefore closely superimpose. This benefit disappears when a heating stage is followed by a cooling stage, as for the H1 and C2 stages, with the result that some probes are lost and the absolute extent of hybridization in the second (i.e., C2) stage decreases. While undesirable, the probe loss did not materially affect determination of thermodynamic parameters. The reason for this lack of impact is illustrated by the normalized data in the inset to Figure 4. Since normalization leads to nearly identical transition profiles, during modeling the decreased hybridization capacity becomes largely accommodated through rescaling of the total probe coverage S_0 rather than through changes in hybridization enthalpy, ΔH_H°, or entropy, ΔS_H°.

3.3. Net/DNA Associations in Solution. Solution isothermal titration calorimetry (ITC) studies provided benchmark data for validation of surface assays. Netropsin was gradually added to solutions of PF/CPF duplexes, whose base sequence is identical to PI/CPI duplexes of the surface assays but without end modifications for immobilization or labeling. In the lowest ionic strength SP150 buffer, the evolved heat of binding demonstrated a dip, Figure 5. This distinct feature, as

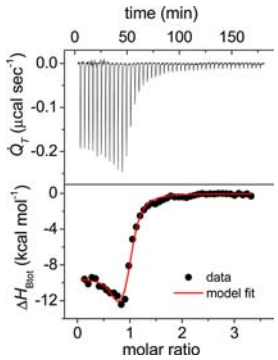

Figure 5. Isothermal titration calorimetry data. Top: Rate of heat evolution ($\dot{Q}_T$) during titration of Net into a solution of PF/CPF duplexes at 19.8 °C in SP150. Bottom: the corresponding binding enthalpy ΔH_{Btot} (points) as a function of the concentration ratio of added Net to duplex. The curve is a fit to a two-site model with the parameters listed in Table 2.

in prior reports,[39,81,82] is interpreted to reflect formation of two complexes: one in which Net fits into the minor groove in a curved conformation, and a second in which the drug is more linear and a bridging water molecule compensates the resultant incompatibility with groove curvature.[81,82] The dip was significantly less pronounced in SP345 and disappeared in SP790, consistent with only a single binding mode at higher salt. In all three buffers, the evolved heat dropped sharply at a 1:1 drug/duplex stoichiometry, indicating binding of one Net per duplex. Therefore, fitting of ITC data was performed under a stoichiometric constraint of $n = 1$ in eq 6, with a two site model used for SP150 and a one site model for SP345 and SP790 data.[81,83]

ITC results are summarized in Table 2. In SP150, the water-bridged association corresponds to mode 2 and the fitted fractions of duplexes in mode 1 and mode 2 binding are denoted by n_1 and n_2, respectively. The derived thermodynamic values are consistent with previous reports in that the water-bridged mode 2 exhibits a more favorable enthalpy offset by negative, unfavorable entropy of binding.[81,82,84] For the investigated sequence, mode 2 disappeared at higher ionic

dx.doi.org/10.1021/ja3066368 | J. Am. Chem. Soc. 2012, 134, 18667−18676

Table 2. Netropsin Binding Thermodynamics in Solution[a,b]

buffer	n[c]	ΔH_B° (cal mol^{-1})	ΔS_B° (cal mol^{-1} K^{-1})	ΔG_B° (cal mol^{-1}) (20 °C)
SP150				
mode 1	0.66 ± 0.09	−9500 ± 300	5.2 ± 2.7	−11,000
mode 2	0.34 ± 0.12	−16200 ± 3700	−23.8 ± 13	−9,200
SP345	1	−8900 ± 200	3.5 ± 0.7	−9,900
SP790	1	−9900 ± 200	−2.7 ± 0.9	−9,100

[a]PF/CPF duplex, 19.8 °C. [b]n, ΔH_B°, and ΔS_B° are the stoichiometry, standard enthalpy change, and standard entropy change of binding. For SP150, two values are listed because of two distinct binding modes. [c]For all buffers, n ($n = n_1 + n_2$ for SP150) was fixed at 1.

strengths; this suggests that attrition of electrostatic interactions (e.g., between the positive Net and DNA phosphates) favors mode 1 over mode 2. For mode 1, ΔS_B° became less favorable at higher ionic strength while no clear dependence was apparent for ΔH_B°. A more favorable binding entropy at low ionic strengths, as in prior reports,[49,85] can be attributed at least partly to release of bound Na^+ counterions from the duplex due to binding of the positively charged Net.[85] Because the resultant entropic gain diminishes with increase in solution concentration of Na^+, ΔS_B° decreases at higher salt and, eventually, becomes negative as expected for an association interaction in the absence of offsetting factors.

3.4. Net/DNA Binding on Solid Supports. *3.4.1. Summary.* Surface assays were performed as a function of ionic strength and Net concentration. For each combination of conditions, a complete melting cycle, consisting of a cooling followed by a heating stage, was first performed in the absence of Net to characterize duplex stability. This "cycle I" was followed by a second cool/heat cycle, "cycle II" in a fresh solution with added Net, to observe the resultant effect on the melting transition. In one series of experiments, the Net concentration was raised from 5 to 2000 nmol L^{-1} in SP150 buffer, Figure 6A. In a second series of experiments, Figure 6B, netropsin concentration was held at 2000 nmol L^{-1} while the buffer varied between SP150, SP345, and SP790.

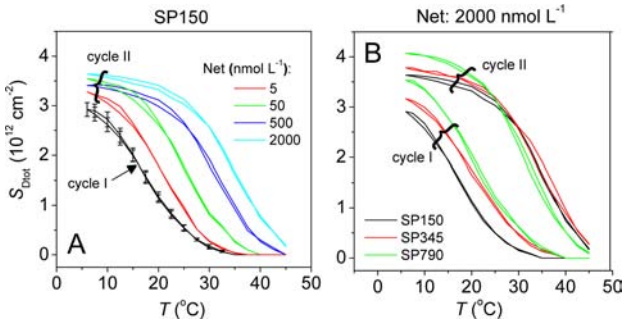

Figure 6. Surface melting transitions for PI/CPI duplexes. (A) In SP150 buffer as a function of Net concentration. To decrease crowding of the curves, the cycle I curve is an average of traces measured for the four Net concentrations. (B) For a fixed Net concentration of 2000 nmol L^{-1}, as a function of buffer ionic strength.

Addition of Net increased the melting temperatures T_m, indicating that complexation with netropsin stabilized the duplex state. Increasing the Net concentration in the SP150 buffer, Figure 6A, produced T_m shifts from 2.5 °C for 5 nmol L^{-1} up to 18 °C for the 2000 nmol L^{-1} Net concentration. There was no evidence of dual binding modes, observed in ITC, in the melting data; this is consistent with duplexes cycling between both modes as they melt, thus resulting in equivalent melting profiles. Increasing the buffer ionic strength while keeping Net concentration fixed at 2000 nmol L^{-1} caused both cycle I (no Net) and cycle II (with Net) transitions to shift, Figure 6B. The combined effect was a decreased T_m shift from Net binding at higher salt, dropping from 18 °C in SP150 to just 12 °C in SP790. This decrease indicates that stabilization by Net weakens with ionic strength, implying an electrostatic contribution to the Net-duplex attraction. Indeed, as documented by solution studies[85−87] and, for our specific sequence, by the ITC results in Table 2, the binding affinity of the 2+ charged Net for duplex DNA decreases with ionic strength due to increasingly unfavorable entropy of binding.

3.4.2. Modeling Considerations. A central approximation of most models of DNA melting, including the model of section 2.6, is two-state behavior in which only fully melted or fully hybridized structures are considered.[88] This two-state assumption is expected to be reasonable for the short 9mer sequences used because short sequences are less prone to formation of complex, partially hybridized arrangements. Use of short sequences for ligand association studies is not overly restrictive as most small molecule ligands interact with less than 6 base pairs. The model also assumed that enthalpy and entropy of hybridization (ΔH_H° and ΔS_H°), as well as of small molecule binding (ΔH_B° and ΔS_B°), are independent of temperature; in other words, that heat capacity changes accompanying these binding processes are negligible.[89,90] If desired heat capacity effects could be incorporated through additional parameters; introduction of more parameters, however, should first be motivated by inability of the simpler model to account for experimental observations. In line with this approximation, Fiche et al.[73] have previously estimated that, in their surface melting experiments, heat capacity effects fell within experimental uncertainty.

Examination of surface melting curves (e.g., Figure 6) also shows that, at low temperatures, S_{Dtot} continued to gradually increase with decreasing temperature rather than reaching a steady value. This trend may reflect presence of difficult-to-hybridize probes that do not bind with complements until sufficiently low temperatures are reached. Such probes may be, for example, in sterically frustrated conformations (e.g., due to proximity to other probes) for which only partial duplexes, involving less than 9 base pairs, can form. Impact of the low temperature data on estimation of thermodynamic parameters was assessed by analyzing melt transitions both with and without a low-temperature "baseline correction" (section 3.4.3).

Lastly, the enthalpy and entropy of binding can exhibit significant correlation during fitting because, over the fairly narrow temperature window of a melting transition, enthalpic and entropic variations can partly offset one another in the free energy $\Delta G^\circ = \Delta H^\circ - T\Delta S^\circ$ from which the melting transition is calculated (cf. eqs 4 through 7). This correlation can, in principle, be decoupled by simultaneously fitting multiple melt

transitions corresponding to different Net concentrations, as considered below for the SP150 Net concentration series.

3.4.3. Comparison of Surface and Solution Thermodynamics. The enthalpy and entropy of Net−DNA association were derived in SP150 buffer by fitting to the data of Figure 6A. Agreement of predicted, via eqs 6 (cycle II) and 7 (cycle I), melting transitions with experimental curves was optimized by minimizing the least-squares error through adjustment of S_0, ΔH_H°, ΔS_H°, ΔH_B° and ΔS_B°. Provided that the state (e.g., aggregation) of Net in solution and of the binding environment inside the minor groove do not vary with Net concentration, ΔH_B° and ΔS_B° should remain the same; accordingly, the same ΔH_B° and ΔS_B° were assumed to apply to all four Net concentrations. However, since experiments at different Net concentrations were run on independently prepared electrodes, with expected differences in probe coverage, S_0 was allowed to vary between melting curves; moreover, because S_0 is known to impact hybridization thermodynamics,[60,66,91,92] ΔH_H° and ΔS_H° were also allowed to vary independently for each melting curve.

Calculations were performed both without and with a low temperature baseline correction for which S_0 in eqs 6 and 7 was replaced by a linearly decreasing function, $S_0 = b - mT$, as a simplest model of a temperature-dependent coverage of hybridizable probes. The m parameter was chosen to fit the limiting slope at low temperatures observed under the highest (2000 nmol L^{-1}) Net concentration, since this concentration afforded the widest regime for judging the low temperature asymptotic behavior. The b intercept was optimized for each trace during fitting. The inset in Figure 7 illustrates the low-temperature baseline correction graphically, while the main panel shows examples of fits with (green curves) and without (red curves) the low-temperature baseline. Use of the baseline produced visually better agreement at low temperatures, especially in the presence of Net (cycle II data) for which the low temperature limiting response was more obvious.

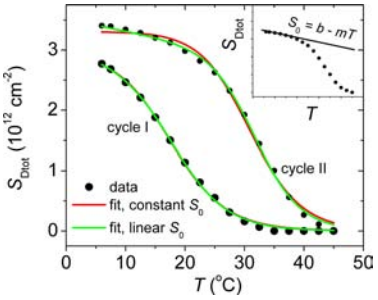

Figure 7. Main panel: Comparison of model fits based on eqs 6 (cycle II) and 7 (cycle I) to experimental data, for 2000 nmol L^{-1} Net concentration. Fitting was performed both without (red curves) and with (green curves) a low temperature baseline correction. Inset: Illustration of the baseline correction, which assumes a linear variation in coverage of active probes S_0 with temperature.

As shown in the third row of Table 3, free energies ΔG_B° from surface and solution assays were in excellent agreement, irrespective of how the coverage S_0 of hybridizable probes was treated, constant or linearly dependent on temperature. This result provides an important initial validation of surface denaturation assays, and more specifically of robustness of ΔG_B° as a quantitative metric for assessing DNA/ligand interactions. The similarity in free energy, whether or not duplexes were immobilized, moreover suggests that the minor groove microenvironment was not dramatically perturbed by tethering to a solid support. A more definitive comparison of surface and solution results, in terms of interaction energies and dispersal over molecular degrees of freedom, would require ΔH_B° and ΔS_B°; however, unlike ΔG_B°, derivation of these values depended significantly on treatment of S_0. While Table 3 shows that assumption of a linear variation of S_0 with T successfully reproduced ITC results for ΔH_B° and ΔS_B°, more extensive studies across multiple sequences and binding ligands are needed to validate a general approach. The present analysis does suggest, however, that it will be necessary to account for changes in the coverage of hybridizable probes with temperature.

The enthalpies and entropies of hybridization, ΔH_H° and ΔS_H° in Table 3, are seen to be lower in absolute magnitude at the surface than in solution. This decrease agrees with trends discussed elsewhere,[94−96] and confirms that differences between surface and solution hybridization require independent measurement of ΔH_H° and ΔS_H°. In particular, predictive algorithms designed for solution environments[56,97] may prove misleading when applied to surface situations.

A characteristic feature of binding by charged ligands, such as netropsin, is dependence of binding affinity on ionic strength. For a ligand with valency Z interacting with double-stranded DNA in presence of monovalent salt cations M, theory[98,99] predicts $d \ln K_B / d \ln C_M \approx -Z\psi$, where $\ln K_B = -\Delta H_B^\circ/RT + \Delta S_B^\circ/R$ is the equilibrium constant, C_M is the solution concentration of M, and ψ is the counterion binding parameter describing association of the M cations with DNA due to counterion condensation and screened electrostatic interactions. For long double-stranded DNA, $\psi = 0.88$;[98] thus, for divalent Net ligands, theory predicts $d \ln K_B / d \ln C_M = -1.76$. Experimental values of $d \ln K_B / d \ln C_M$ range from −0.8 to −1.8, with values near −1 typical for oligonucleotides while more negative values, closer to the theoretical prediction, observed for polymeric DNA.[87]

Table 4 and Figure 8 compare the ionic strength dependence of $\ln K_B$ at the surface, evaluated at 30 °C, with that from solution ITC measurements. For the surface data, $d \ln K_B / d \ln C_{Na+} = -1.2$, in reasonable agreement with −1.3 derived from ITC as well as with −1.0 reported by Rentzeperis et al. for a different duplex with an AATT recognition site.[87] Also in agreement with prior studies, the experimental $d \ln K_B / d \ln C_{Na+}$ is significantly less than the theoretically predicted −1.76. This difference from theory is not surprising. As in the solution studies employing oligonucleotides, the short duplexes of the present report are expected to have weakened associations with counterions relative to polymeric DNA because of end effect corrections;[100] moreover, at the high ionic strengths used (i.e., $a/r_D \approx 1$, where a is the cylinder radius and r_D the Debye screening length) a more appropriate structural model for DNA is that of a "thick cylinder"[101] which has weaker counterion associations than the "line of charges" on which the prediction $\psi = 0.88$ is based. In addition to these expected sources of deviation, the weaker experimental dependence of $\ln K_B$ on $\ln C_{Na+}$ may reflect offsetting effects of Net binding. For example, while charge compensation from binding of positively charged Net may release some DNA counterions into solution, the binding also stabilizes double-stranded structure what may reduce thermal fraying at duplex ends, an effect that could favor counterion retention.

dx.doi.org/10.1021/ja3066368 | J. Am. Chem. Soc. 2012, 134, 18667−18676

Table 3. Results of the Net Concentration Series in SP150 (Figure 6A)

parameter	surface: constant S_0	surface: linear S_0-T dependence	solution
		DNA/Net Binding	
ΔH_B° (cal mol^{-1})	−9,500 ± 1,500[a]	−12,000 ± 700[a]	−11,800[b]
ΔS_B° (cal mol^{-1} K^{-1})	3.0 ± 4.7[a]	−4.7 ± 2.3[a]	−4.7[b]
ΔG_B° (cal mol^{-1}) (30 °C)	−10,420 ± 50[c]	−10,510 ± 30[c]	−10,400[c]
		Hybridization	
ΔH_H° (cal mol^{-1})	−37,400 ± 1,100[a]	−37,700 ± 1,200[a]	−71,200 ± 5,000[d]
ΔS_H° (cal mol^{-1} K^{-1})	−93.7 ± 3.3[a]	−94.5 ± 3.5[a]	−203 ± 16[d]
ΔG_H° (cal mol^{-1}) (30 °C)	−9,000 ± 100[c]	−9,000 ± 100[c]	−9,600 ± 100[c]

[a]These values are averages and standard deviations from fits to cooling as well as to heating stages of melt curves. For both the cooling and heating series, five trials starting from different initial guesses were used, and the results were averaged.[93] [b]From ITC data, Table 2. Mode 1 and mode 2 values were combined using $\Delta X_B^\circ = n_1\Delta X_{B,1}^\circ + n_2\Delta X_{B,2}^\circ$ where n_i is the mode stoichiometry and ΔX is ΔH or ΔS. [c]$\Delta G^\circ = \Delta H^\circ - T\Delta S^\circ$ were calculated for each trial fit, then averaged. [d]From solution melting curves of PF/CPF duplexes. Values are averages of four measurements.

Table 4. Results of the Ionic Strength Series for 2000 nmol L^{-1} Net concentration (Figure 6B)

buffer	lnK_B (30 °C, surface)	lnK_B (30 °C, solution)
SP150	17.1 ± 0.1[a]	17.2[b]
SP345	16.0 ± 0.2[a]	16.5[b]
SP790	15.1 ± 0.1[a]	15.1[b]

[a]Values are averages and standard deviations derived from cooling and heating stages. [b]From solution ITC results in Table 2. For SP150, mode 1 and mode 2 values were combined according to $\Delta X_B^\circ = n_1\Delta X_{B,1}^\circ + n_2\Delta X_{B,2}^\circ$, where n_i is the mode stoichiometry and ΔX is ΔH or ΔS used to calculate lnK_B at the temperature of interest.

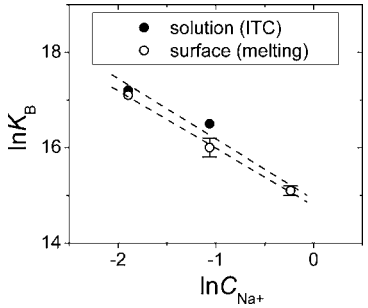

Figure 8. Dependence of Net/DNA binding affinity, K_B, on counterion concentration, C_{Na+}. Points, data; lines, linear fits. The slopes are −1.3 and −1.2 for ITC and surface melting data, respectively.

4. CONCLUSIONS

Multiplexing of assays on solid supports offers scalability for analysis of molecular interactions, combined with frugality of reagent consumption. However, the interfacial environment also brings significant challenges. These challenges include, among others, confirmation of equilibrium for thermodynamic analyses, stability of the surface system during measurement, and potential complications from altered interactions due to mutual proximity of surface-confined molecules.

This study adapted a solution technique for thermodynamic analysis of interactions between DNA and small molecules to a surface format. In this approach, binding thermodynamics are extracted from ligand-induced differences in the stability of short, surface-tethered DNA duplexes, as quantified from their thermal melting profiles. Using netropsin as a reversibly binding small molecule with a sequence-specific DNA affinity, these studies reach the following principal conclusions: (1) DNA melting assays on solid supports can provide information on free energies of DNA/ligand interactions of comparable quality to solution assays, including recovery of ionic strength dependencies; (2) reliable extraction of enthalpies and entropies of binding will require, at a minimum, better understanding of hybridization yields in the low temperature limit (i.e., below the main melting transition) as part of implementing appropriate baseline corrections; (3) reversibility of measurement can be rigorously confirmed from superposition of cooling and heating traces so long as scan rates are properly adapted to the surface melting kinetics (e.g., slowed strand dissociation rates at lower ionic strengths); and (4) conventional tethering of DNA via monovalent thiolate-type bonds to gold with mercaptohexanol passivation exhibits sufficient thermostability for surface melting measurements up to about 45 °C; at higher temperatures, more robust immobilization methods are expected to be required.

■ ASSOCIATED CONTENT

Supporting Information

Estimation of upper limits on partitioning energies $E_{P,Net}$. This material is available free of charge via the Internet at http://pubs.acs.org.

■ AUTHOR INFORMATION

Corresponding Author

rlevicky@poly.edu

Notes

The authors declare no competing financial interest.

■ ACKNOWLEDGMENTS

This work was supported by the National Science Foundation under Awards No. DMR 07-06170 and DMR 12-06754, and by the National Institutes of Health under Award No. R01HG004512.

■ REFERENCES

(1) Gottesfeld, J. M.; Neely, L.; Trauger, J. W.; Baird, E. E.; Dervan, P. B. *Nature* **1997**, *387*, 202.
(2) Melander, C.; Burnett, R.; Gottesfeld, J. M. *J. Biotechnol.* **2004**, *112*, 195.
(3) Mapp, A. K.; Ansari, A. Z. *ACS Chem. Biol.* **2007**, *2*, 62.
(4) Nelson, S. M.; Ferguson, L. R.; Denny, W. A. *Mutat. Res.* **2007**, *623*, 24.
(5) Schaal, T. D.; Mallet, W. G.; McMinn, D. L.; Nguyen, N. V.; Sopko, M. M.; John, S.; Parekh, B. S. *Nucl. Acids. Res.* **2003**, *31*, 1282.
(6) Haq, I. *Arch. Biochem. Biophys.* **2002**, *403*, 1.
(7) Hiraku, Y.; Oikawa, S.; Kawanishi, S. *Nucl. Acids. Res. Suppl.* **2002**, *2*, 95.

(8) Denissenko, M. F.; Pao, A.; Tang, M. S.; Pfeifer, G. P. *Science* **1996**, *274*, 430.
(9) Anders, M. W. *Chem. Res. Toxicol.* **2008**, *21*, 145.
(10) Hecht, S. S. *Chem. Res. Toxicol.* **2008**, *21*, 160.
(11) Hang, B. *J. Nucleic Acids* **2010**, *2010*, 1.
(12) Reddy, B. S. P.; Sondhi, S. M.; Lown, J. W. *Pharmacol. Ther.* **1999**, *84*, 1.
(13) Baraldi, P. G.; Bovero, A.; Fruttarolo, F.; Preti, D.; Tabrizi, M. A.; Pavani, M. G.; Romagnoli, R. *Med. Res. Rev.* **2004**, *24*, 475.
(14) van Rijt, S. H.; Sadler, P. J. *Drug Discovery Today* **2009**, *14*, 1089.
(15) Cortesi, R.; Esposito, E. *Min. Rev. Med. Chem.* **2010**, *10*, 218.
(16) van Lanen, S. G.; Shen, B. *Curr. Top. Med. Chem.* **2008**, *8*, 448.
(17) Torres, F. E.; Recht, M. I.; Coyle, J. E.; Bruce, R. H.; Williams, G. *Curr. Opin. Struct. Biol.* **2010**, *20*, 598.
(18) Boger, D. L.; Fink, B. E.; Brunette, S. R.; Tse, W. C.; Hedrick, M. P. *J. Am. Chem. Soc.* **2001**, *123*, 5878.
(19) Tse, W. C.; Boger, D. L. *Acc. Chem. Res.* **2004**, *37*, 61.
(20) Glass, L. S.; Bapat, A.; Kelley, M. R.; Georgiadis, M. M.; Long, E. C. *Bioorg. Med. Chem. Lett.* **2010**, *20*, 1685.
(21) Hauschild, K. E.; Stover, J. S.; Boger, D. L.; Ansari, A. Z. *Bioorg. Med. Chem. Lett.* **2009**, *19*, 3779.
(22) Warren, C. L.; Kratochvil, N. C. S.; Hauschild, K. E.; Foister, S.; Brezinski, M. L.; Dervan, P. B.; Phillips, G. N.; Ansari, A. Z. *Proc. Natl. Acad. Sci. U.S.A.* **2006**, *103*, 867.
(23) Puckett, J. W.; Muzikar, K. A.; Tietjen, J.; Warren, C. L.; Ansari, A. Z.; Dervan, P. B. *J. Am. Chem. Soc.* **2007**, *129*, 12310.
(24) Ho, D.; Dose, C.; Albrecht, C. H.; Severin, P.; Falter, K.; Dervan, P. B.; Gaub, H. E. *Biophys. J.* **2009**, *96*, 4661.
(25) Bischoff, G.; Bischoff, R.; Birch-Hirschfeld, E.; Gromann, U.; Lindau, S.; Meister, W. V.; Bambirra, S. D.; Bohley, C.; Hoffmann, S. *J. Biomol. Struct. Dyn.* **1998**, *16*, 187.
(26) Wong, C.-H.; Hendrix, M.; Manning, D. D.; Rosenbohm, C.; Greenberg, W. A. *J. Am. Chem. Soc.* **1998**, *120*, 8319.
(27) Wang, L.; Bailly, C.; Kumar, A.; Ding, D.; Bajic, M.; Boykin, D. W.; Wilson, W. D. *Proc. Natl. Acad. Sci. U.S.A.* **2000**, *97*, 12.
(28) Wolf, L. K.; Fullenkamp, D. E.; Georgiadis, R. M. *J. Am. Chem. Soc.* **2005**, *127*, 17453.
(29) Nguyen, B.; Tanious, F. A.; Wilson, W. D. *Methods* **2007**, *42*, 150.
(30) Redman, J. E. *Methods* **2007**, *43*, 302.
(31) Pope, L. H.; Allen, S.; Davies, M. C.; Roberts, C. J.; Tendler, S. J. B.; Williams, P. M. *Langmuir* **2001**, *17*, 8300.
(32) Yang, M. S.; Yau, H. C. M.; Chan, H. L. *Langmuir* **1998**, *14*, 6121.
(33) Breslauer, K. J.; Remeta, D. P.; Chou, W.-Y.; Ferrante, R.; Curry, J.; Zaunczkowski, D.; Snyder, J. G.; Marky, L. A. *Proc. Natl. Acad. Sci. U.S.A.* **1987**, *84*, 8922.
(34) Crothers, D. M. *Biopolymers* **1971**, *10*, 2147.
(35) Wilson, W. D.; Tanious, F. A.; Fernandez-Saiz, M.; Rigl, C. T. *Methods Mol. Biol.* **1994**, *90*, 219.
(36) Zimmer, C.; Reinert, K. E.; Luck, G.; Wahnert, U.; Lober, G.; Thrum, H. *J. Mol. Biol.* **1971**, *58*, 329.
(37) Finlay, A. C.; Hochstein, F. A.; Sobin, B. A.; Murphy, F. X. *J. Am. Chem. Soc.* **1951**, *73*, 341.
(38) Zimmer, C.; Wahnert, U. *Prog. Biophys. Mol. Biol.* **1986**, *47*, 31.
(39) Lewis, E. A.; Munde, M.; Wang, S.; Rettig, M.; Le, V.; Machha, V.; Wilson, W. D. *Nucleic Acids Res.* **2011**, *39*, 9649.
(40) Dolenc, J.; Gerster, S.; van Gunsteren, W. F. *J. Phys. Chem. B* **2010**, *114*, 11164.
(41) Premvardhan, L.; Maurizot, J. C. *Eur. Biophys. J.* **2010**, *39*, 781.
(42) Andac, C. A.; Miandji, A. M.; Hornemann, U.; Noyanalpan, N. *Int. J. Biol. Macromol.* **2011**, *48*, 531.
(43) Thewes, R.; Hofmann, F.; Frey, A.; Schienle, M.; Paulus, C.; Schindler-Bauer, P.; Holzapfl, B.; Brederlow, R. *Advanced Micro & Nanosystems. Vol. I. Enabling Technology for MEMS and Nanodevices*; Wiley VCH Verlag GmbH & Co.: Weinheim, Germany, 2004; Vol. *1*.
(44) Augustyniak, M.; Paulus, C.; Brederlow, R.; Persike, N.; Hartwich, G.; Schmitt-Landsiedel, D.; Thewes, R. *IEEE Int. Solid State Circuits Conf. Dig.* **2006**, 59.
(45) Levine, P. M.; Gong, P.; Levicky, R.; Shepard, K. L. *IEEE J. Solid-State Circuits* **2008**, *43*, 1859.
(46) Levine, P. M.; Gong, P.; Levicky, R.; Shepard, K. L. *Biosens. Bioelectron.* **2008**, *24*, 1995.
(47) Kruppa, P.; Frey, A.; Kuehne, I.; Schienle, M.; Persike, N.; Kratzmueller, T.; Hartwich, G.; Schmitt-Landsiedel, D. *Biosens. Bioelectron.* **2010**, *26*, 1414.
(48) Zimmer, C. *Prog. Nucleic Acid Res. Mol. Biol.* **1975**, *15*, 285.
(49) Marky, L. A.; Blumenfeld, K. S.; Breslauer, K. J. *Nucleic Acids Res.* **1983**, *11*, 2857.
(50) Oesch, U.; Janata, J. *Electrochim. Acta* **1983**, *28*, 1237.
(51) Herne, T. M.; Tarlov, M. J. *J. Am. Chem. Soc.* **1997**, *119*, 8916.
(52) Levicky, R.; Herne, T. M.; Tarlov, M. J.; Satija, S. K. *J. Am. Chem. Soc.* **1998**, *120*, 9787.
(53) Tercero, N.; Wang, K.; Gong, P.; Levicky, R. *J. Am. Chem. Soc.* **2009**, *131*, 4953.
(54) McGhee, J. D. *Biopolymers* **1976**, *15*, 1345.
(55) The solution concentrations of Net and complement strands were in 100-fold or higher excess.
(56) SantaLucia, J. *Proc. Natl. Acad. Sci. U.S.A.* **1998**, *95*, 1460.
(57) Fuchs, J.; Fiche, J. B.; Buhot, A.; Calemczuk, R.; Livache, T. *Biophys. J.* **2010**, *99*, 1886.
(58) Okahata, Y.; Kawase, M.; Niikura, K.; Ohtake, F.; Furusawa, H.; Ebara, Y. *Anal. Chem.* **1998**, *70*, 1288.
(59) Peterson, A. W.; Wolf, L. K.; Georgiadis, R. M. *J. Am. Chem. Soc.* **2002**, *124*, 14601.
(60) Gong, P.; Levicky, R. *Proc. Natl. Acad. Sci. U.S.A.* **2008**, *105*, 5301.
(61) Vainrub, A.; Pettitt, B. M. *Phys. Rev. E* **2002**, *66*, No. art 041905.
(62) Vainrub, A.; Pettitt, B. M. *Biopolymers* **2003**, *68*, 265.
(63) Halperin, A.; Buhot, A.; Zhulina, E. B. *Biophys. J.* **2004**, *86*, 718.
(64) Halperin, A.; Buhot, A.; Zhulina, E. B. *J. Phys.: Condens. Matter* **2006**, *18*, S463.
(65) Wong, I. Y.; Melosh, N. A. *Biophys. J.* **2010**, *98*, 2954.
(66) Irving, D.; Gong, P.; Levicky, R. *J. Phys. Chem. B.* **2010**, *114*, 7631.
(67) Donnan, F. G. *J. Membr. Sci.* **1995**, *100*, 45.
(68) Li, Z.; Jin, R.; Mirkin, C. A.; Letsinger, R. L. *Nucleic Acids Res.* **2002**, *30*, 1558.
(69) Johnson, P. A.; Levicky, R. *Langmuir* **2003**, *19*, 10288.
(70) Johnson, P. A.; Gaspar, M. A.; Levicky, R. *J. Am. Chem. Soc.* **2004**, *126*, 9910.
(71) Lai, R. Y.; Seferos, D. S.; Heeger, A. J.; Bazan, G. C.; Plaxco, K. W. *Langmuir* **2006**, *22*, 10796.
(72) Dougan, J. A.; Karlsson, C.; Smith, W. E.; Graham, D. *Nucleic Acids Res.* **2007**, *35*, 3668.
(73) Fiche, J. B.; Buhot, A.; Calemczuk, R.; Livache, T. *Biophys. J.* **2007**, *92*, 935.
(74) Sakata, T.; Maruyama, S.; Ueda, A.; Otsuka, H.; Miyahara, Y. *Langmuir* **2007**, *23*, 2269.
(75) Civit, L.; Fragoso, A.; O'Sullivan, C. K. *Electrochem. Commun.* **2010**, *12*, 1045.
(76) Phares, N.; White, R. J.; Plaxco, K. W. *Anal. Chem.* **2009**, *81*, 1095.
(77) Sharma, J.; Chhabra, R.; Yan, H.; Liu, Y. *Chem. Commun.* **2008**, 2140.
(78) Ge, D.; Wang, X.; Williams, K.; Levicky, R. *Langmuir* **2012**, 28.
(79) Bloomfield, V. A.; Crothers, D. M.; Tinoco, I; Jr. *Nucleic Acids—Structures, Properties, and Functions*; University Science Books: Sausalito, CA, 2000.
(80) Ge, D.; Levicky, R. *Chem. Commun.* **2010**, *46*, 7190.
(81) Degtyareva, N. N.; Fresia, M. J.; Petty, J. T. *Biochemistry* **2007**, *46*, 15136.
(82) Freyer, M. W.; Buscaglia, R.; Cashman, D.; Hyslop, S.; Wilson, W. D.; Chaires, J. B.; Lewis, E. A. *Biophys. Chem.* **2007**, *126*, 186.
(83) Freyer, M. W.; Lewis, E. A. *Methods Cell Biol.* **2008**, *84*, 79.
(84) Cooper, A. *Biophys. Chem.* **2005**, *115*, 89.
(85) Marky, L. A.; Breslauer, K. J. *Proc. Natl. Acad. Sci. U.S.A.* **1987**, *84*, 4359.

(86) Rentzeperis, D.; Marky, L. A. *J. Am. Chem. Soc.* **1993**, *115*, 1645.
(87) Rentzeperis, D.; Marky, L. A.; Dwyer, T. J.; Geierstanger, B. H.; Pelton, J. G.; Wemmer, D. E. *Biochemistry* **1995**, *34*, 2937.
(88) Puglisi, J. D.; Tinoco, I. J. *Methods Enzymol.* **1989**, *180*, 304.
(89) Breslauer, K. J.; Sturtevant, J. M.; Tinoco, I. J. *J. Mol. Biol.* **1975**, *99*, 549.
(90) Mikulecky, P. J.; Feig, A. L. *Biopolymers* **2006**, *82*, 38.
(91) Steel, A. B.; Herne, T. M.; Tarlov, M. J. *Anal. Chem.* **1998**, *70*, 4670.
(92) Lee, C. Y.; Nguyen, P. C. T.; Grainger, D. W.; Gamble, L. J.; Castner, D. G. *Anal. Chem.* **2007**, *79*, 4390.
(93) Typical variation in $\chi 2$ between fits was 20%.
(94) Watterson, J. H.; Piunno, P. A. E.; Wust, C. C.; Krull, U. J. *Langmuir* **2000**, *16*, 4984.
(95) Xu, J.; Craig, S. L. *J. Am. Chem. Soc.* **2005**, *127*, 13227.
(96) Chen, C. L.; Wang, W. J.; Ge, J.; Zhao, X. S. *Nucleic Acids Res.* **2009**, *37*, 3756.
(97) Markham, N. R.; Zuker, M. In *Bioinformatics, Vol. II. Structure, Functions and Applications*; Keith, J. M., Ed.; Humana Press: Totowa, NJ, 2008; Vol. *453*, p 3.
(98) Record, M. T.; Anderson, C. F.; Lohman, T. M. *Q. Rev. Biophys.* **1978**, *11*, 103.
(99) Manning, G. S. *Q. Rev. Biophys.* **1978**, *11*, 179.
(100) Manning, G. S.; Mohanty, U. *Physica A* **1997**, *247*, 196.
(101) Manning, G. S. *J. Phys. Chem. B.* **2007**, *111*, 8554.